ACTA METALLURGICA SLOVACA
2023, VOL. 29, NO. 2, 108-112

RESEARCH PAPER

Mg_2Si INTERMETALLIC ALLOYS: PHASE GROWTH AND MICROSTRUCTURE

Septian Adi Chandra[1], Rahadian Roberto[1], Dedi Pria Utama[1], Dhany Zulkarnain[1], Delfiarina Salsabila Putri Bratawan[2], Mila Saprila Suherman[2], Annisfiah Gayatri[2], Arif Tjahjono[2], Muhammad Yunan Hasbi[1], Sigit Dwi Yudanto[1]

[1]*Research Center for Metallurgy, National Research and Innovation Agency, Banten, 15314, Indonesia*
[2]*Department of Physics, Faculty of Sciences and Technology, UIN Syarif Hidayatullah Jakarta, Banten, 15412, Indonesia*

*Corresponding author: sigi012@brin.go.id & sd.yudanto@gmail.com, tel.: +6281213024663

Received: 03.05.2023
Accepted: 06.06.2023

ABSTRACT

The Mg_2Si intermetallic alloys have been prepared by using a powder metallurgy process. The milling treatment of silicon powder as a raw material to improve the formation of the Mg_2Si phase was investigated in this research. The un-milled and milled silicon powder was mixed with magnesium powder and milled for 2 hours. The milled powders were compacted in stainless steel tubes and sintered at 500 and 600°C for 6 hours. The phase formation and crystal structure were identified using the X-ray diffractometer (XRD), while the fracture surface was observed under the scanning electron microscope (SEM). The XRD results show that the Mg_2Si phase is the dominant phase, with the highest mass fraction of 86.31%. The lattice parameter calculated from the Mg_2Si cubic phase is 0.6355 nm. As a result, we might derive the conclusion that the Mg_2Si intermetallic alloys can be produced with atmospheric mechanical milling under air and powder sintering techniques in a tube.

Keywords: intermetallic; Mg_2Si; powder metallurgy; milling; lattice

INTRODUCTION

Since the combustion process produces thermal energy, it is an energy source that can be converted to electrical energy. The material required for conversion shall have thermo-electrical characteristics. Materials with thermoelectric properties generate electricity when two conductors differ in temperature [1]. A general property of thermoelectric is the operating of thermocouples via the Seebeck effect. The value of the figure of merit (ZT) indicates that a material can be used as a thermoelectric. Thermoelectric materials of type p and n are two different types used to construct thermoelectric modules, which are combined with each other.

Mg_2Si – an intermetallic alloy with a cubic crystal structure (Fm-3m) atomic site coordinates of Mg (1/4,1/4,1/4) and Si (0,0,0) [2] has an excellent opportunity to be applied as a thermoelectric with an operating temperature range of 300 – 600°C [3, 4]. The lattice a-constant of the Mg_2Si crystal structure is 0.6356 nm, and the Mg-Mg bond length=0.319 nm [5–8]. The ZT value of Mg_2Si alloy continues to increase through doping with certain elements [9, 10]. Tani et al. reported that the ZT value of Bi-doped Mg_2Si at the Si site was 0.86 at 589°C [11]. **Fig. 1** shows the crystal structure of Mg_2Si.

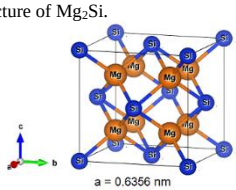

Fig. 1 Mg_2Si crystal structure (adapted from Mizoguchi et al. [5], Hayashi, et al [2], and constructed using Vesta [12])

While there have been many efforts to improve the performance of Mg_2Si-based materials, a number of researchers are still developing their synthesis methods [13–17]. The synthesis method used by several researchers and efforts to increase the formation of the Mg_2Si phase. Stathokostopoulos et al. offered a pack cementation method for the synthesis of Mg_2Si-based materials [13, 18]. They mixed Mg and Si powders with variations of Mg/Si ratio and added NH_4Cl as the powder activator. The mixed powder was put into a crucible and heated at 500 and 650°C for 3 – 4 hours while flowing argon gas [18]. Based on X-ray diffraction (XRD) analysis, they claim that the sample with a ratio of Mg/Si=2.18 which was heated at 650°C for 4 hours produced the highest Mg_2Si phase with less magnesium oxide [18]. The absence of Mg and Si phase in the sample proves that the excess Mg plays a role in compensate the levels of oxidized Mg.

To prevent the formation of magnesium oxide, the synthesis of the Mg_2Si intermetallic alloy was carried out under the melting temperature of magnesium. As done by Zhang et al., they compared the raw materials of Mg and MgH_2 powders in the synthesis of Mg_2Si [14]. Mg_2Si alloys through solid-state reaction method with low formation temperature and minimal MgO obtained with MgH_2 as raw material [14]. However, there has been no research using the milling method in free air conditions and heating in a closed tube during the sintering process. In this study, we investigated the effect of free-air milling and sintering processes that utilize stainless steel tubing on the formation of Mg_2Si-based intermetallic alloy. In addition, the influence of the initial milling of silicon powder was also observed.

MATERIAL AND METHODS

Materials preparation

Synthesis of Mg_2Si alloys using magnesium powder (purity 98.5%) and Si powder (purity 99%). Mg_2Si intermetallic alloy was synthesized by using the powder metallurgy process. The raw silicon powder with no pre-milling and milling for 2 hours are compared in order to investigate its effect to the formation of the Mg_2Si alloy. Weighing the Mg and Si powders with an atomic ratio of Mg:Si=2:1 was the first step in the synthesis, which was done in line with the Mg-Si phase diagram [19]. Subsequently, the powders were placed in a stainless-steel vial and the steel balls were then added with a ball-to-powder ratio (BPR) of 2:1. The two powders were mixed and then milled using a shaker mill for 2 hours. The milled powders were poured in the stainless-steel tube and sealed at both ends of the tube to prevent oxidation during the sintering process. This sealed technique was used in previous Mg-based material research [20, 21]. The stainless-steel tube containing the mixed powder was heated for 6 hours at temperatures of 500 and 600°C to produce the Mg_2Si phase. The heating process occurs in the air atmosphere, while the cooling process is performed naturally in a furnace. The sample codes are tabulated in **Table 1**.

Materials characterization

A Rigaku Smart Lab XRD with Cu Kα radiation (λ=0.15406 nm) was used to identify the phase and crystal structure. The operating parameters were 36 mA, 36 kV, 0.01° steps, and a range of 2θ = 10 - 90°. The phase composition and crystal parameters were determined from the diffraction patterns using the Rietveld method [22]. Scanning electron microscope (SEM) JEOL JSM-6390A was used to observe the fracture surface morphology of the samples. After the sintering process, the bulks were mechanically removed from the tube. Using secondary electrons, the surface morphology of the bulk flakes was inspected.

Table 1 Mg_2Si-based alloys sample code

Sample code	Si-powder treatment	T_{sinter} (°C)	t_{sinter} (hours)
MS1-500	Milled, 2 hours	500	6
MS1-600	Milled, 2 hours	600	6
MS2-500	Un-milled	500	6
MS2-600	Un-milled	600	6

RESULTS AND DISCUSSION

XRD analysis

In this study, to determine the effect of the initial milling of powder raw materials on the formation of Mg_2Si alloys, the silicon powder was ground with a shaker mill for 2 hours. The comparison of the diffraction pattern of silicon powder before and after milling is shown in **Fig. 2**. In the inset **Fig. 2**, it can be seen that there is a widening of the peaks and a decrease in the intensity of the diffraction pattern of milled silicon powder, indicated by a dashed line. Broadening and decreasing the intensity of the peaks indicate a reduction in the grain size of the silicon powder. **Fig. 3a-b** shows the diffraction pattern of the Mg_2Si-based alloy samples powder after being removed from the stainless-steel tube and ground using an agate mortar. All peaks indexed at (111), (200), (220), (311), (222), (400), (331), (420), (422), and (511) in the four samples are reflections of the Mg_2Si phase [6, 17], [23]. Si, Mg, MgO, and SiO_2 phase were found in the alloy samples. M. Saleemi et al. reported that the results of Mg_2Si preparation using the planetary ball mill method still showed Si and MgO impurity phases [17]. According to them, this unreacted Si is the result of the formation of MgO. So that the ratio of formation of Mg_2Si alloy is not fulfilled according to the phase diagram of the Mg-Si system. Based on the Mg-Si phase diagram, the Mg_2Si phase will form when the atomic ratio Mg/Si=2 [19]. Stathokostopoulos et al. conducted experiments with variations in the Mg/Si ratio. They made an effort to minimize unreacted silicon by exaggerating the amount of magnesium [18]. In contrast to the work done by Nakhowong et al., a single phase Mg_2Si was obtained by solid state reaction method by heating 800°C for 6 hours under argon conditions reported by Nakhowong et al [23]. When compared with the results of previous reports, the results we obtained with the simple method offered have the same tendency.

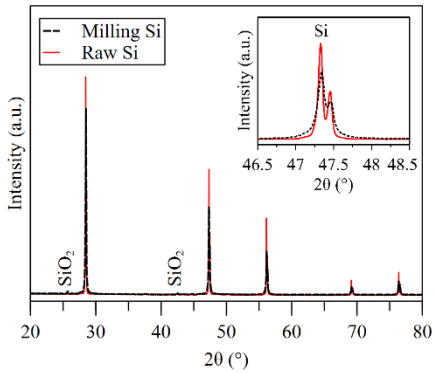

Fig. 2 Diffraction pattern of raw and milling silicon powder. The insert image shows the magnification of the peak angle of 2θ 47.35°, the solid red line represents raw Si, and the black dashed line represents milling Si.

The MgO phase at 42.77° and 62.15° shows that oxidation is still taking place during the synthesis. The MgO phase is the default phase of the raw material and can also be formed during the milling process in free air conditions [17]. However, in general, the sintering process in a closed tube has been shown to eliminate the formation of MgO. As shown in the inset images in **Fig. 3a** and **3b**, it can be seen that the peak intensity of the Si phase at an angle of 28.47° decreased with the increase in the sintering temperature. In addition, the peak intensity of the Si phase in the samples using Si-milled powder was lower than the Si powder without milling. This indicates an increase in the formation of the Mg_2Si phase.

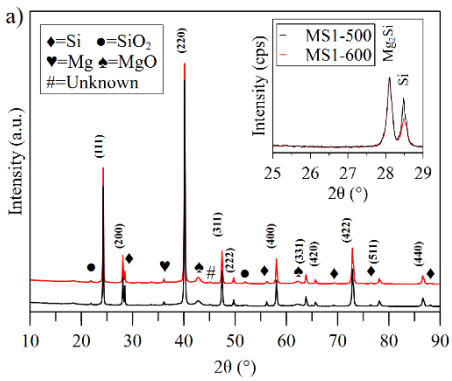

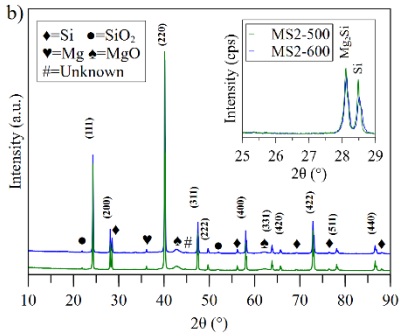

Fig. 3 Powder XRD of the Mg_2Si-based alloy samples at room temperature, a). Sample MS1-500 and MS1-600, and b). Sample MS2-500 and MS2-600

Based on the qualitative analysis of the diffraction pattern in **Fig. 3a** and **3b**, the synthesis results still show multiphase. A quantitative analysis was carried out using the Rietveld method to estimate the composition of the phase. The comparison of the diffraction patterns calculated and observed for the samples MS1-500, MS1-600, MS2-500, and MS2-600 is shown in **Fig. 4 a–d**. Calculation of the composition of the formed phase refers to the Mg_2Si, Si, Mg, MgO, and SiO_2 phase as well as the results of a qualitative analysis. Samples generated with Si powder that was milled for 2 hours and sintered at 600°C produced the highest Mg_2Si phase of 86.31 wt.%. Sunohara et al. reported an increase in the formation of the Mg_2Si phase in direct proportion to the refinement of silicon particles [24]. **Table 2** shows that the increase in the mass fraction of the Mg_2Si phase was not only due to the milling treatment of silicon powder but also to the increase in sintering temperature. Isoda et al. stated that the sintering time was above 4 hours capable of heating to 870°C [15]. They also reported that single phase Mg_2Si was easily obtained using silicon with a size below 53 µm.

Table 2 Quantitative analysis of diffraction, lattice parameters, and inter-atomic bond length calculation results of Mg_2Si-based alloy samples

Parameter	MS1-500	MS1-600	MS2-500	MS2-600
Mg_2Si, wt.%	82.45	86.31	72.99	77.92
Impurities, wt.%	17.55	13.69	27.01	22.08
a-lattice, nm	0.6354	0.6355	0.6353	0.6355
Mg-Mg bond length, nm	0.3176	0.3177	0.3176	0.3177
Mg-Si bond length, nm	0.2751	0.2751	0.2751	0.2751
Density, g/cm^3	1.986	1.985	1.986	1.985

The refined lattice parameters of the Mg_2Si-based samples are tabulated in **Table 2**, along with the composition of the phases that were formed. The lattice parameters for samples based on Mg_2Si heated at 600°C obtained a value of 0.6355 nm. The value of this lattice parameter has similarities with the results reported by Hayashi et al [2].

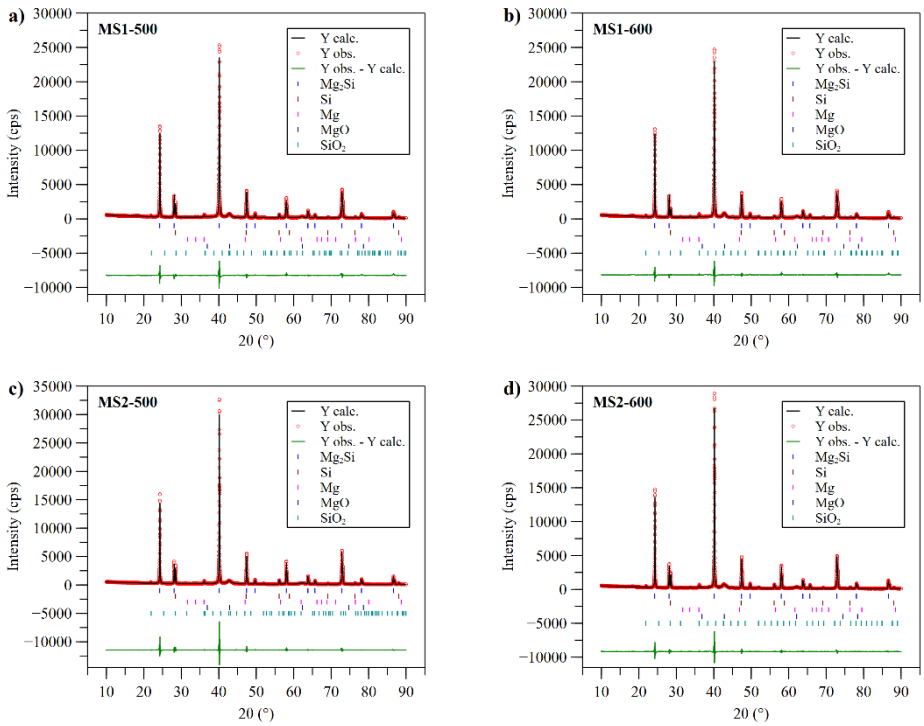

Fig. 4 The calculated curve results of the diffraction pattern of the Mg_2Si-based alloys sample powder. a). MS1-500, b). MS1-600, c). MS2-500, and d). MS2-600

SEM analysis

Fig. 5 shows the observations of the surface microstructure of samples MS1-600 and MS2-600. Granules with heterogenous shapes and non-uniform sizes existed in the MS1-600 sample. The granules of the MS2-600 sample appear to have a more homogeneous shape with a larger size than the MS1-600 sample. This is consistent with the XRD peak intensity of the sample MS2-600, which was higher than that of MS1-600 (**Fig. 4b** and **4d**).

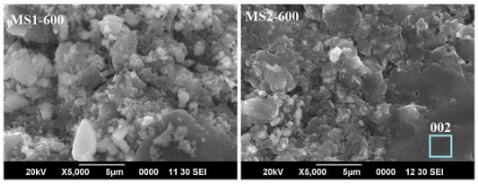

Fig. 5 Secondary Electron (SE) image of the fracture surface of the sample MS1-600 and MS2-600

Fig. 6 shows the elemental composition of the fracture surface area 002 of sample MS2-600. In the inset of **Fig. 6**, it can be seen that the atomic ratio of Mg:Si=2.04:1. This elemental ratio approximates the value of the ratio in the phase diagram of the Mg-Si system. Hu et al. reported that the average atomic ratio of Mg and Si elements from the EDS test results of Mg_2Si-based samples prepared by the spark plasma sintering (SPS) method was 2.11 [23].

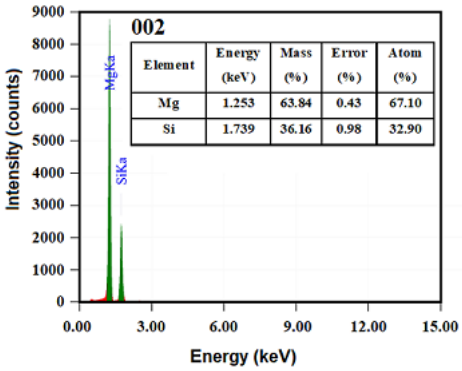

Fig. 6 Energy curves and elemental composition of the energy dispersive X-ray spectroscopy (EDS) test of sample MS2-600 in area 002 (**Fig. 5**)

In addition, the fracture surfaces of both the MS1-600 and MS2-600 samples (**Fig. 5**) exhibit cleavage facets indicating fracture of sintered agglomerates. This shows that the sintering temperature of 600°C is high enough for recrystallization of Mg_2Si-based material.

CONCLUSIONS

The synthesis of Mg_2Si intermetallic alloy has been successfully carried out through the powder metallurgy process. The highest mass fraction of the Mg_2Si phase of 86.31% was obtained in samples prepared with milled Si powder as raw material, which was then ground with magnesium powder and sintered at 600°C for 6 h. Si, Mg, MgO, and SiO_2 phase are identified phases other than the Mg_2Si phase. The cubic Mg_2Si phase has lattice a-constant value of 0.3655 nm.

Acknowledgments: We thank National Research and Innovation Agency for funding this research through the Rumah Program Material Maju - OR Nanotechnology and Materials 2022 scheme under contract No. 7/III/HK/2022. We also thank the Deputy for Research and Innovation Infrastructure for the research equipment and characterization facilities in the KST B. J. Habibie, South Tangerang, Banten, Indonesia.

REFERENCES

1. I. Terasaki: Introduction to thermoelectricity. In: *Materials for Energy Conversion Devices*. Woodhead Publishing Series in Electronic and Optical Materials, Cambridge: Woodhead Publishing, 2005, p. 339–357. https://doi.org/10.1533/9781845690915.3.339.
2. K. Hayashi, W. Saito, K. Sugimoto, K. Ohoyama, K. Hayashi, N. Happo, M. Harada, K. Oikawa, Y. Inamura, Y. Miyazaki: AIP Advances, 10(3), 2020, 035115. https://doi.org/10.1063/1.5143839.
3. D. Shiojiri, T. Iida, N. Hirayama, Y. Imai, H. Sugawara, J. Kusaka: Energies, 15, 2022, p. 4859. https://doi.org/10.3390/en15134859.
4. H. Inoue, S. Yoneda, M. Kato, I. J. Ohsugi, T. Kobayashi: Journal of Alloys and Compounds, 735, 2018, 828–832. https://doi.org/10.1016/j.jallcom.2017.11.202.
5. H. Mizoguchi, Y. Muraba, D. C. Fredrickson, S. Matsuishi, T. Kamiya, H. Hosono: Angewandte Chemie - International Edition, 56, 2017, 1–6. https://doi.org/10.1002/anie.201701681.
6. M. Ioannou, G. Polymeris, E. Hatzikraniotis, A. U. Khan, K. M. Paraskevopoulos, T. Kyratsi: Journal of Electronic Materials, 42(7), 2013, pp. 1827–1834. https://doi.org/10.1007/s11664-012-2442-6.
7. K. Kutorasinski, B. Wiendlocha, J. Tobola, S. Kaprzyk: Physical Review B - Condensed Matter and Materials Physics, 89, 2014, 115205. https://doi.org/10.1103/PhysRevB.89.115205.
8. G. Kim et al.: Journal of Alloys and Compounds, 801, 2019, 234–238. https://doi.org/10.1016/j.jallcom.2019.06.075.
9. M. Cahana, Y. Gelbstein: Intermetallics, 120, 2020, 106767. https://doi.org/10.1016/j.intermet.2020.106767.
10. X. J. Tan, W. Liu, H. J. Liu, J. Shi, X. F. Tang, C. Uher: Physical Review B, 85, 2012, 205212. https://doi.org/10.1103/PhysRevB.85.205212.
11. J. I. Tani, H. Kido: Physica B, 364, 2005, 218–224. https://doi.org/10.1016/j.physb.2005.04.017.
12. K. Momma, F. Izumi: Journal of Applied Crystallography, 44, 2011, 1272–1276. https://doi.org/10.1107/S0021889811038970.
13. D. Stathokostopoulos et al.: Physica Status Solidi (A) Applications and Materials Science, 211, 2014, 1308–1314. https://doi.org/10.1002/pssa.201300140.
14. F. Zhang, Q. Meng, W. Fan, S. Chen, D. Zhang: Procedia Engineering, 27, 2012, 200–205. https://doi.org/10.1016/j.proeng.2011.12.444.
15. Y. Isoda, S. Tada, N. Shioda, Y. Shinohara: Journal of Alloys and Compounds, 656, 2016, 598–603. https://doi.org/10.1016/j.jallcom.2015.07.291.
16. M. Nanko et al.: in IOP Conference Series: Materials Science and Engineering, 2011, p. 012006. https://doi.org/10.1088/1757-899X/21/1/012006.
17. M. Saleemi et al.: Journal of Materials Science, 48, 2013, 1940–1946.

https://doi.org/10.1007/s10853-012-6959-0.
18. D. Stathokostopoulos et al.: Results in Materials, 13, 2022, 100252. https://doi.org/10.1016/j.rinma.2021.100252.
19. H. Okamoto: Journal of Phase Equilibria and Diffusion, 28, 2007, 229–230. https://doi.org/10.1007/s11669-007-9038-5.
20. S. D. Yudanto et al.: Journal of Superconductivity and Novel Magnetism, 32, 2019, 2829–2835. https://doi.org/10.1007/s10948-019-5061-0.
21. S. D. Yudanto et al.: Journal of Metals, Materials and Minerals, 30(3), 2020, 9–14. https://doi.org/10.14456/jmmm.2020.32.
22. A. C. Larson, R. B. Von Dreele: Los Alamos National Laboratory Report, 2004, p. 1–224.
23. C. Nakhowong, T. Sumpao, T. Seetawan: Advanced Materials Research, 802, 2013, pp. 213–217. https://doi.org/10.4028/www.scientific.net/AMR.802.213.
24. K. Sunohara et al.: in Materials Research Society Symposium Proceedings, 2015, pp. 1–6. https://doi.org/10.1557/opl.2015.